# Defense Technical Information Center Compilation Part Notice

# ADP011112

TITLE: Active Flow Control Activities at Onera

DISTRIBUTION: Approved for public release, distribution unlimited

## This paper is part of the following report:

TITLE: Active Control Technology for Enhanced Performance Operational Capabilities of Military Aircraft, Land Vehicles and Sea Vehicles [Technologies des systemes a commandes actives pour l'amelioration des performances operationnelles des aeronefs militaires, des vehicules terrestres et des vehicules maritimes]

To order the complete compilation report, use: ADA395700



The following component part numbers comprise the compilation report:
ADP011101 thru ADP011178

# Active Flow Control Activities at Onera

**J-L Gobert, D.Barberis, T.Mitchell, P.Molton, J-P Archambaud, G.Pailhas, M.Corrège**

ONERA
2, avenue Edouard Belin - F31055 Toulouse Cedex

Paper n°14 presented at the AVT SYMPOSIUM on
Active Control Technology for Enhanced Performance Operation Capabilities of Military Aircraft, Land Vehicles and Sea Vehicles
Braunschweig, Germany, 8-11 May 2000

**SUMMARY** : In 1997, O.N.E.R.A (French National Aerospace Research Establishment) created a multidisciplinary project on the subject of active flow control. Experimental work, computational fluid dynamic studies, modelling and synthesis of control laws constitute the main activities of this project. The investigations include laminarity control, buffet control in transonic conditions and control of separated flows and vortices.

This document presents the results obtained during some of these activities.

**RESUME** : En 1997, l'Office National d'Etudes et de Recherches Aérospatiales (O.N.E.R.A) a décidé de créer un projet interne réunissant des spécialistes de plusieurs disciplines sur le sujet du contrôle actif d'écoulements aérodynamiques. Ce projet inclut des travaux expérimentaux ainsi que des recherches en modélisation d'écoulements et synthèse de lois de contrôle. Les thèmes retenus sont ceux du contrôle de la laminarité, du contrôle de tremblement en conditions transsoniques et du contrôle des décollements et tourbillons.

Ce document présente quelques résultats obtenus dans certaines de ces activités.

## 1. INTRODUCTION

The natural instabilities of the flow which appear on aerospace vehicle surfaces are a source of energy dissipation increasing drag and producing noise and vibrations, therefore they have prejudicial consequences on the performances.

Competitive pressures are pushing civil aircraft designers towards low-cost solutions and some compromises have to be accepted leading to wing designs slightly different from the "optimum". Increased traffic around airports also leads to flight regimes outside of the design operating point.

Demands for more manoeuvrability and stealth are pushing military aircraft designers to develop new concepts for the control of separation and of vortices on the nose and wings at high angle of attack.

Active flow control might be a solution to these different problems.

In order to deal with these problems, ONERA has decided in 1997 to establish an internal project on this subject. The main goal is to build a staff including engineers from all of the required disciplines : experimental and theoretical aerodynamics, control theory, control design and implementation, actuator, sensor, ....

The basic idea is that a small and localised action (local deformation, suction, blowing, jet, ...) can sufficiently modify global parameters of the flow (lift, drag, symmetry, ...) with little energy consumption to considerably improve the situation.

In this document, the activities performed at ONERA are briefly presented :

1- Control of Tollmien-Schlichting waves in a laminar boundary layer
2- Control of the 3D separation caused by a wing-body junction,
3- Control of the 3D separation on an ellipsoid-cylinder model,
4- Control of Vortex breakdown on a Delta wing.

Other activities performed on active control of buffet and side force control on a generic forebody at high angle of attack are presented in other documents [1,2].

## 2. TOLLMIEN-SCHLICHTING WAVES CONTROL

The so-called Tollmien-Schlichting (TS) waves are the primary instabilities leading to the transition from laminar to turbulent flow. A study with the objective to control these waves started end of 1997 at ONERA. The main goal is to get a better understanding of the mechanism driving the TS waves and to try to develop a technique cancelling or at least reducing considerably them as soon as they start to grow.

TS wave cancellation is a quite complex problem. For that reason, it has been decided to study a simplified configuration. It consists in developing a system able to cancel one or a group of monochromatic waves on a flat plate with a zero pressure gradient. The control is based on the wave superposition principle: a counter disturbance is applied at a given point with the detected frequency and the appropriate phase and amplitude in such a way that the resulting signal will be zero.

The purpose of this paper is to describe the principle of the technique used and to present some examples of results [3,4].

### 2.1. EXPERIMENTAL SETUP

The experiments are carried out in a low speed wind tunnel equipped with a test section of 300mm high, 400mm wide and 1 100mm long. The freestream

velocity is equal to 12ms$^{-1}$ with a turbulence level close to 0.5%.

An aluminium horizontal flat plate, 780mm

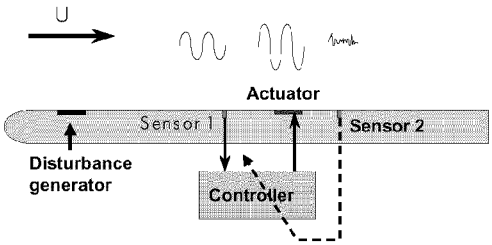


Fig.1: Flat plate instrumentation

long, is installed in the middle of the test section. The instrumentation mounted on the flat plate is shown on fig.1. A disturbance generator is installed under the surface of the flat plate, near the leading edge, producing a quasi-sine wave of adjustable frequency. This wave is an artificial TS which is convected by the fluid movement. Further the disturbance is measured on the flat plate surface by a sensor (hot film). This signal is

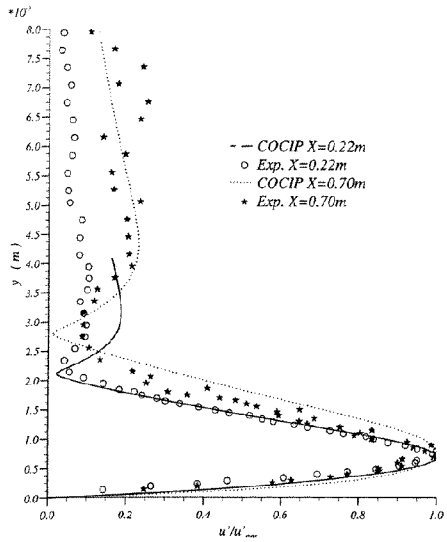


Fig.2: Comparison of experimental and theoretical stream-wise velocity fluctuation profiles

used by the controller to detect the wave frequency and to optimise the parameters sent to the actuator in order to cancel the initial disturbance. Downstream of the actuator, a second sensor measures the result of the TS manipulation ; this information can be used by the controller to compute a correction factor applied to the process.

In order to check the functioning of the disturbance generator and to characterise in detail the flow field around the flat plate, a hot wire probe can be moved in the x (longitudinal) and y (transversal) directions.

### 2.2. QUALIFICATION OF THE GENERATED DISTURBANCE

The natural boundary layer on the flat plate is laminar from the leading edge down to the trailing edge. In a first phase, a computation based on the boundary layer stability theory using a code developed at ONERA Toulouse (COCIP) [3] indicated that the frequencies of the most unstable waves range from 100Hz to 120Hz. So the generator will be excited within that range during the experiments in order to work in the most critical conditions.

As very first result, the stream-wise velocity recorded at several locations in the boundary layer shows that the instabilities appear on the form of sine waves as predicted by the theory. Moreover, fluctuation profiles measured with the hot wire probe at two stations (just behind the generator and close to the end of the flat plate) are compared to computed profiles (COCIP code) in the fig.2. The agreement between theory and experiment shall be highlighted.

In conclusion, the generated wave can be considered as a good representation of a TS wave.

### 2.3. CONTROL PROCEDURE

The control procedure is based on the relation:

$$U_a(t) = -K U_c(t-r)$$

where $U_a$ – command signal to the actuator,
$U_c$ = signal measured by the upstream sensor,
$K$ = gain factor,
$r$ = phase shift
$K$ and $r$ are the unknowns of the problem.

In a first step, the control system is operating in open loop. For a range of disturbance frequencies, the effect of the actuator is optimised in terms of best couple of values (gain factor, phase shift). All the final results are compiled in a data base.

During real tests, the control system operates in closed loop. The first sensor measures the incoming disturbance. A numeric filter analyses this input, detects the TS wave and extracts from the data base the relevant values of the parameters which are sent to the actuator. Then the residual instability is measured downstream of the actuator by the second sensor, allowing to qualify the actual action of the control.

### 2.4. EXAMPLES OF RESULTS

#### *2.4.1. Monochromatic TS wave*

The first tests have consisted in cancellation of monochromatic waves in the range of the most unstable frequencies. So TS waves of discrete frequency values (110, 120, 130, 140 and 150Hz) have been excited. The feedback control system has given a fairly good attenuation of the TS wave for all these frequencies except the highest value 150Hz. Fig.3 shows the result for 120Hz. On the left side, is drawn the incoming disturbance exhibiting a sharp peak of energy corresponding to the excited frequency. On the right side, are compared the open and closed loop modes are compared; the TS waves have been efficiently cancelled in both the cases.

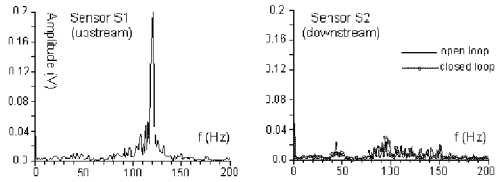


Fig.3: Cancellation of a TS wave (f = 120 Hz)

### 2.4.2. *Chromatic TS wave*

In the boundary layer, many fluctuations of different frequencies are superposed; they are amplified or damped independently in the linear amplification zone and finally they lead to the transition. Consequently some tests have been performed with a chromatic generated disturbance. Fig.4 presents the example of an excited frequency range within 100 and 150 Hz. On the left hand side are plotted the signal of the incoming disturbance (above) and the corresponding spectrum (below). On the right hand side are plotted the same variables measured downstream of the actuator by the second sensor. We can observe that the signal amplitude is strongly reduced and not well organised (above) and that remains only a small spot of energy between 140 and 150 Hz.

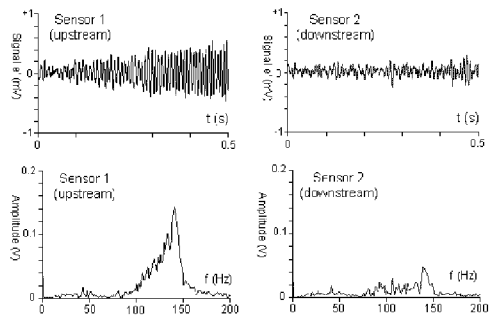


Fig.4: Cancellation of a TS wave (f = 120 Hz)

### 2.4.3. *Control influence on the amplitude of the flow fluctuations along the flat plate*

Then, investigations have been conducted to measure the influence of the control on the amplitude of the fluctuations contained into the boundary layer. For these investigations, the hot wire has been moved along the stream-wise axis, at 0.6 mm from the plate surface, which approximately corresponds to the location of the maximum velocity fluctuation. Fig.5 shows the fluctuation spectra measured at three stations and for two frequency values, with and without control. In the case of f=130 Hz it can be notice the strong reduction due to the control of the fluctuation amplitudes of all the frequencies. On the contrary, the control has practically no action for f=150 Hz. In the previous paragraph we have already noted that the attenuation just behind the actuator was not complete around this frequency. The reason is that the 150 Hz excited fluctuation causes a very unstable situation, some turbulent spots appearing just behind the actuator and being convected along the plate. In this case the actuator is no more efficient.

The effect of the actuator can also be seen through the modification of the total energy of the

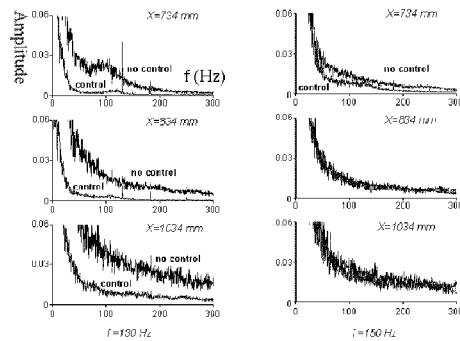


Fig.5: Spectra of the hot wire signal at three stations along the flat plate with/without control

fluctuation spectra previously considered. Fig.6 shows the evolution of this energy along the plate axis for different frequencies of TS waves. Obviously the energy is strongly reduced by the control on the entire plate length and for the different frequencies except for 150 Hz for which no reduction occurs. Nevertheless it can be remarked that the reduced level of energy (with control) seems to grow again but moderately behind X=800 mm. So we can imagine that a second actuator could be placed at this location in order to continue the action of the first one.

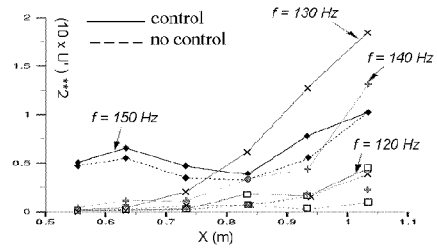


Fig.6: Energy levels along the flat plate with/without control

### 2.4.4. *Effect of the TS control on the position of the transition*

The final objective of the TS manipulation is to move the transition back. In our case the transition is not completely located on the flat plate which is too short. Nevertheless the tendency of the transition movement can be estimated by considering the local intermittency factor. This factor is roughly estimated as the ratio of turbulent spot duration over total duration of the signal sample measured by the hot wire probe (0.6 mm from the plate surface) at several stations. Fig.7 shows the evolution of the intermittency factor for 3 TS frequencies :130, 140 and 150 Hz. For 130 and 140 Hz, the level of the intermittency factor is reduced by the control and the shift of the first turbulent spot appearance can be estimated approximately to $\Delta X = +0.15$ m. For limit frequency of 150 Hz, the situation is globally unchanged with and without control.

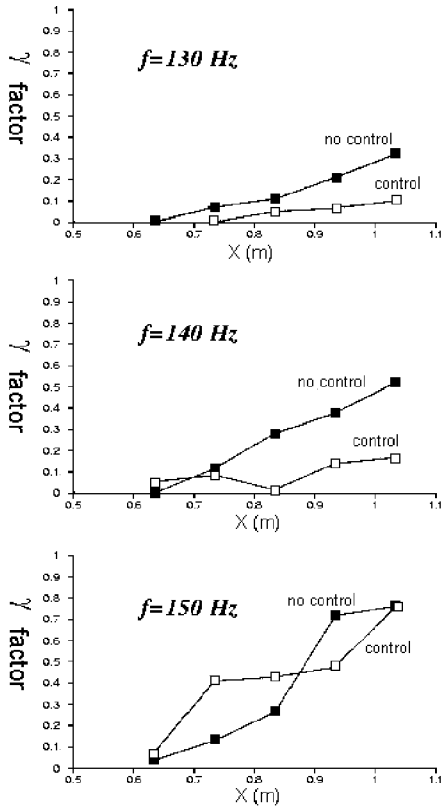


Fig.7: Energy levels along the flat plate with/without control

### 2.4.5. *Use of a second actuator*

A second actuator has been placed at x=800mm, 300mm behind the first one; it is equipped with its own sensors. Fig.8 presents the signals measured in front and behind the first actuator (above) and the analogous results for the second actuator (below). The incoming TS wave is generated at f=140 Hz. The fairly good efficiency of the first actuator is clearly pointed out by the reduction of the amplitude of the signal. The signal which is measured just upstream of the second actuator has a small amplitude and is not very periodic. In this conditions, the controller can not detect a predominant fluctuation and the second actuator has no favourable action. One possibility is that the second actuator has been placed too far from the first one. However, it can be noted that the second actuator provides a small benefit for f=120 Hz, which is less close to the limit of 150 Hz previously mentioned.

### 2.4.6. *Conclusions*

In first conclusion, the production of TS waves by the use of a generator has been demonstrated by comparison of experimental and computed results.

Secondly, a TS control system has been developed, including a reliable set-up and a simplified controller. It has been used in closed loop operation.

The control system has demonstrated a good efficiency in different configurations (monochromatic, chromatic waves). The action of the control on different parameters of the instability has been evaluated. However

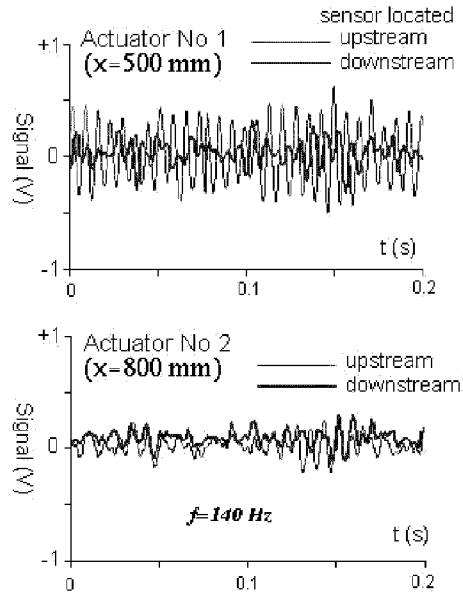


Fig.8: Introduction of a second actuator

a limit of the fluctuation frequency appeared, beyond which the control is invalid.

An attempt to extend the control with a second actuator located behind the first one does not success. Another investigation will be performed with a different configuration.

## 3. CONTROL OF 3D TURBULENT BOUNDARY LAYER SEPARATION AT A WING-BODY JUNCTION

### 3.1. MODEL DEFINITION

For this study, the experimental set-up is made up of a flat plate upon which an obstacle with a circular leading edge is normally mounted. A suction system can be placed in two locations, both consisting of a rectangular opening 100mm wide centred in the plane of symmetry of the flow. The first configuration, with the opening located between X=-184mm and X=-82mm from the obstacle's leading edge, was designed to locate the centre of the opening at the level of the primary separation line. In the second configuration, the suction is located further downstream (between X=-120mm and X=-37mm).

### 3.2. RESULTS

The surface flow properties have been characterised by using a viscous coating which allows the visualisation of the skin friction line patterns. The essential part of the study has been devoted to LDV and PIV measurements. The plane of symmetric flow ahead of the leading edge has been qualified by using 3-D laser

velocimetry in the forward scatter mode and PIV techniques.

### 3.2.1. *Determination of the Aerodynamic Field Using Laser Doppler Velocimeter*

The purpose of this work was to quantify the influence of a suction device on control of separation and vortex development using a simple experimental set-up [5]. In order to examine a large number of configurations in detail, we limited our investigations of the aerodynamic field to the plane of symmetry of the flow upstream of the obstacle's leading edge. The explorations were made for different longitudinal positions in a direction normal to the floor.

### 3.2.2. *Influence of the Suction Rate*

Fig.9 shows the mean velocity vector fields and streamlines obtained in the plane of symmetry of the flow with the suction device located further upstream of the obstacle leading edge. A gradual reduction in the vortex structure size is observed as the suction velocity is increased. Furthermore, as the suction rate increases, the vortex structure moves toward the obstacle leading edge. The turbulent kinetic energy follows the same trend as the vorticity. Its level inside the vortex decreases as the suction rate increases as shown on fig.10.

### 3.2.3. *Influence of the suction device location*

The results obtained with the second configuration at different suction rates are presented on fig.11, which shows the mean velocity fields and associated streamlines. Comparing this figure with the results obtained for the first suction configuration on fig.9 shows that the second arrangement is more efficient in decreasing and eliminating both the separation and the vortex structure observed in the plane of symmetry for the nominal configuration. Indeed, only at Vs = 5 m.s$^{-1}$, do the streamlines no longer show the presence of a vortex. Therefore, from the standpoint of reducing the extent of separation in the plane of symmetry, the objective can be achieved at the lowest suction rates, in opposite to what was observed for the first suction configuration. Fig.12 shows the constant turbulent kinetic energy levels for different suction rates. In the case Vs = 5 m/s, there is a region of high levels of turbulent kinetic energy near the suction opening. For this configuration, the suction rate is sufficient to decrease the size of the vortex, but does not allow complete absorption of the low velocity region originating in the separation point and producing high turbulent kinetic energy levels. At Vs = 10 m.s$^{-1}$, the suction rate is sufficient to absorb the boundary layer at the separation point and eliminate the low velocity region. Finally, above Vs = 10 m.s$^{-1}$, the region located at the junction between the floor and obstacle's leading edge, corresponding to high turbulent kinetic energy levels, gradually decreases and vanishes with the highest suction rate.

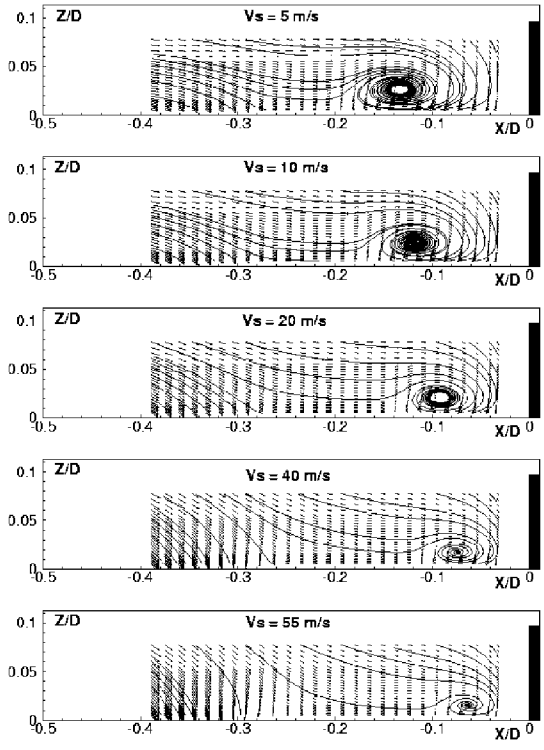


Fig.9 : Mean velocity vector and streamlines:

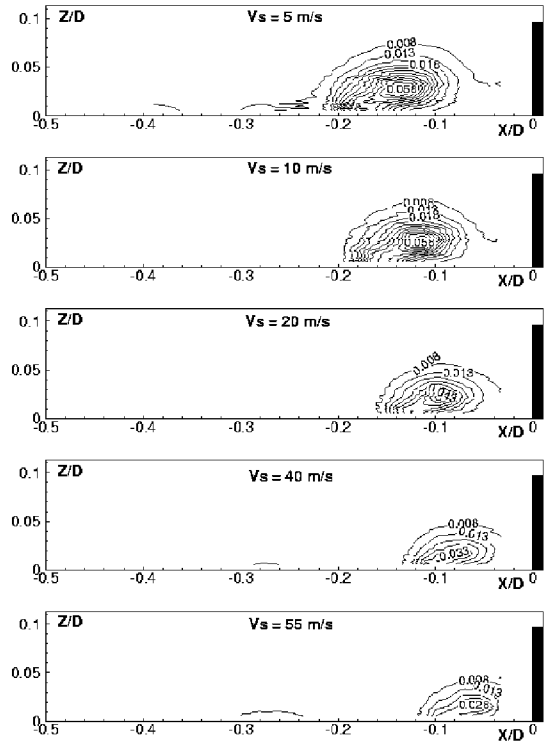


Fig.10: Turbulent kinetic energy:

Suction configuration n°1, plane of symmetry, $V_0$=50m.s$^{-1}$

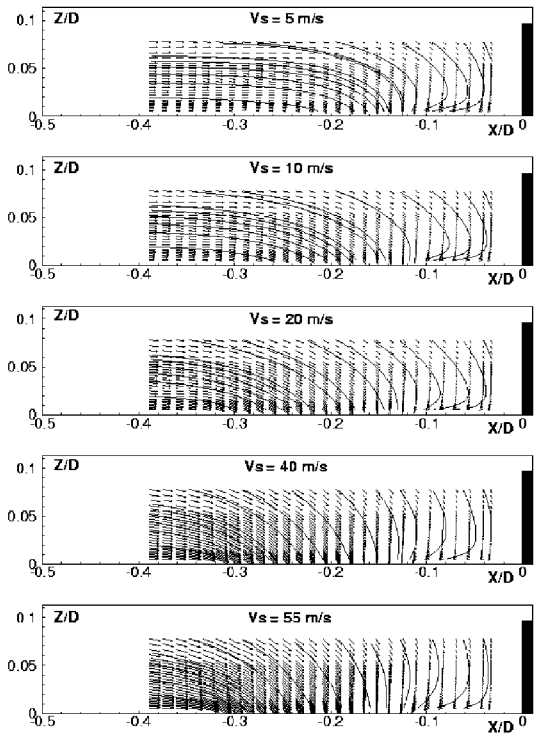


Fig.11: Mean velocity vector and streamlines

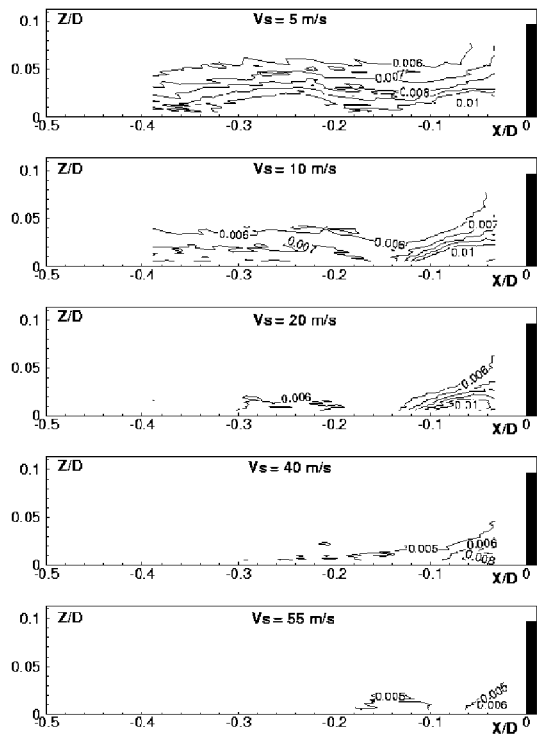


Fig.12: Turbulent kinetic energy

Suction configuration n°2, plane of symmetry, $V_0$=50m.s$^{-1}$

### *3.2.4. Determination of the Aerodynamic Field Using Particle Image Velocimetry*

The instantaneous aerodynamic field was determined by PIV in the symmetry plane of the flow upstream of the obstacle in the nominal configuration, and then in two configurations for flow control.

Fig.13 shows the instantaneous fields obtained by analysis of PIV records, in the form of current line plots. Considerable variation can be observed in the topological structure of the flow in the symmetry plane. In the nominal configuration in particular, the main vortex can break up into more complex structures containing 1, 2 or 3 vortices. Introduction of wall suction

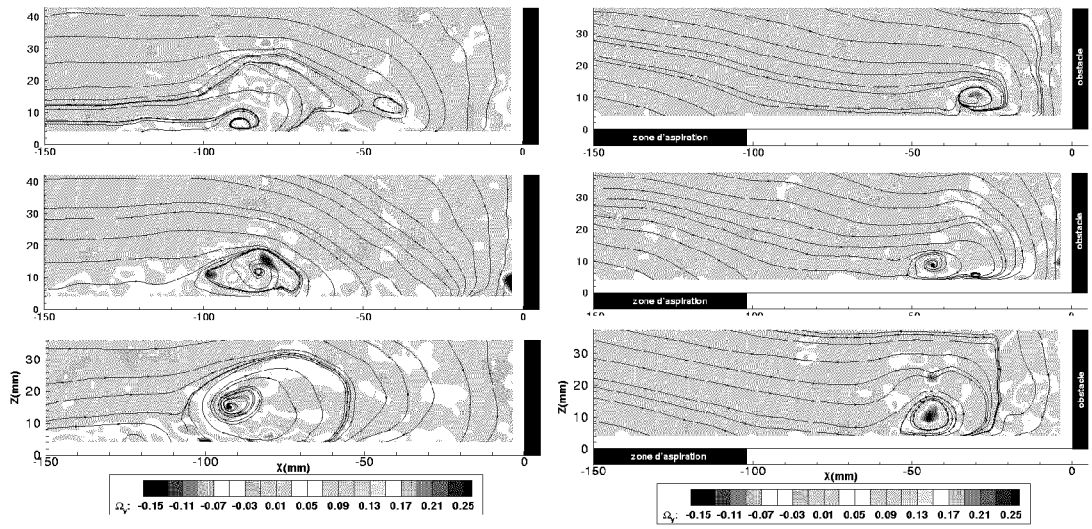


a-nominal configuration

b-configuration with control

Fig.13: Streamlines and iso-rotational values associated with the instantaneous velocity fields obtained by PIV

tends to cause the multiple-vortex topological structures to disappear. From this viewpoint, aspiration appears to stabilise the separation phenomenon.

Analysis of the results should enable construction of model of the vortex system which develops ahead of the leading edge of the obstacle.

## 4. EXPERIMENTAL STUDY OF 3-D SEPARATION CONTROL ON A ELLIPSOID-CYLINDER MODEL

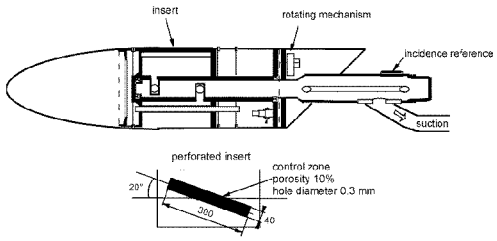


Fig.14: Schematic representation of the model and the suction device

The aim of this work was to study three-dimensional turbulent separation occurring on a regular surface whose radius of curvature was large compared to the thickness of the local boundary-layer.

This problem has already been investigated in detail by focusing on a prolate spheroid with a 1:6 semi-axis ratio. The experiments performed by Meier and Kreplin [6] were extensively exploited. These authors constituted several particularly well documented test cases including wall pressure and wall shear stress measurements as well as detailed flow probing with a multi-hole pressure probe. These experiments were conducted for two incidences : 10° and 30°. Results were obtained for both natural and forced transition; tests at high Reynolds numbers were made in a pressurised wind tunnel [7]

A detailed experimental investigation of vortex formation was performed [8] on a model consisting of a half-oblate ellipsoid followed by a cylinder terminated by a slanted flat base. Surface flow visualisations were made in conjunction with field measurements by five-hole pressure probes and LDV techniques.

The present results are obtained with an axisymmetric model tested in a subsonic wind tunnel. Attention was focused on the boundary-layer evolution in the separation region and the mechanism leading to formation of a clearly detached primary vortex [9]. The flow was investigated in detail using several experimental techniques: surface flow visualisations, surface pressure measurements, field explorations with an LDV system. The objectives of this investigation were to describe the boundary-layer behaviour during three-dimensional separation and to control separation by suction.

### 4.1. Model Definition

The shape of the investigated model has been defined from preliminary tests executed in a water tunnel. It consists of a half axisymmetric prolate ellipsoid with a cylindrical extension terminated by a flat base, inclined at 45° with respect to the model axis, in order to stabilise the separation on the rear part of the obstacle as shown on fig.14. The length, L, of the model between the nose and the middle of the base is equal to 1600 mm. The ellipsoid major axis (A1) is equal to 800 mm while its minor axis (A3) is 200 mm..

### 4.2. Results

Tests were carried out for an upstream velocity of 50m/s and an incidence of 30°. All the tests were conducted with a fixed transition. $XG^1$ represents the distance along the model longitudinal axis measured from the nose. Circumferential angle $\varphi$ has its origin at the windward plane of symmetry ( $\varphi$=0° ) and therefore the leeward plane of symmetry is at $\varphi$=180°. For the presents results, two locations of the suction device have been considered (M = 105° and M = 120° ). The first value corresponds to a position of the control zone just upwind of the origin of the primary separation line and for the second value the suction device is located on the separation line.

#### 4.2.1. *Surface Visualisations*

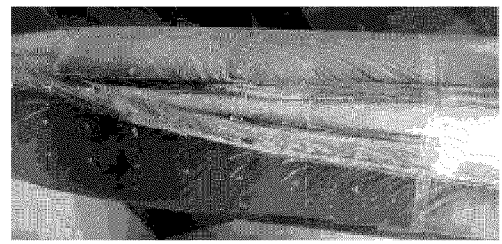

Fig.15: Oil flow visualisation, nominal configuration $\alpha$=30°, $V_0$=50m.s$^{-1}$ , $R_e$=5.6.10$^6$

Fig.16 presents side views of the surface flow patterns obtained for both suction configurations. The suction flow rate was equal to 10 m$^3$/h. These photographs reveal several features common to the two configurations with suction and the side view obtained for the nominal configuration in Fig.15. On the rear part of the model, the skin friction lines coming from the windward plane of symmetry, converge towards a first separation line. Closer to the leeward plane of symmetry, a second separation line is present. The skin friction lines on one side of this separation line come from the leeward plane of symmetry. The picture should be completed by three attachment lines two in the windward and leeward planes of symmetry, one between the two previously mentioned separation lines. From this general description, we can observed some significant differences. The straight secondary separation line observed for the nominal configuration becomes curved on the rear part of

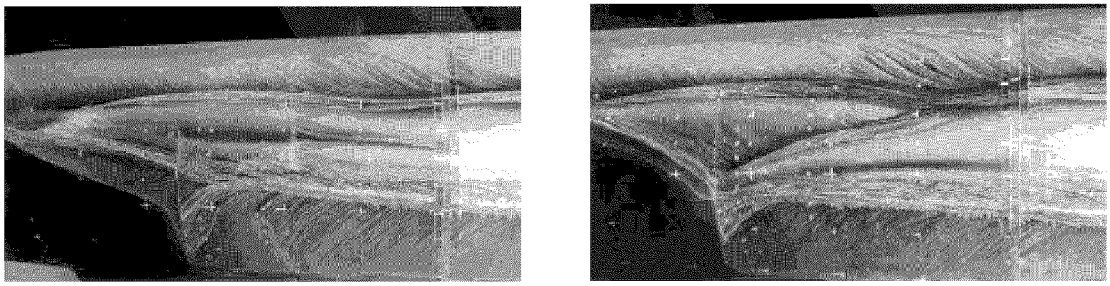

suction at $\Phi$=105° suction at $\Phi$ = 120°

Fig.16: Oil flow visualisations - Suction device location effects
$\alpha$=30° , $V_0$=50m.s$^{-1}$ , Q=10m$^3$.h$^{-1}$ , $R_e$=5.6.10$^6$

the model when suction is applied. This modification is associated with the development of a new separation line. For the configuration with suction at M = 105° this new separation line grows in the area between the primary and secondary separation lines and for the configuration with suction at M = 120°, this line realises a junction between these two lines. In both suction cases, the topological interpretation of the wall visualisations is different from the nominal configuration.

### *4.2.2. Determination of the Aerodynamic Field Using Laser Doppler Velocimeter*

The first section considered is located at $XG^{I'}$ = 1060 mm, just downwind of the control region. The second section, at $XG^{I'}$ = 1300 mm, has been chosen further downstream to quantify the influence of the control at a large distance from the application region.

Fig.17 on the left hand side shows the contours of the longitudinal mean velocity component and streamlines obtained for the nominal configuration, the configuration with suction at M = 105°, and the configuration with suction at M = 120° in the section at $XG^{I'}$ = 1060 mm. For the nominal configuration, the development of a vortex structure is observed. The suction moves the vortex nearer the leeward plane of symmetry, but does not noticeably change its magnitude. In addition, it is observed that in the configurations with suction, a part of the boundary layer is absorbed and the

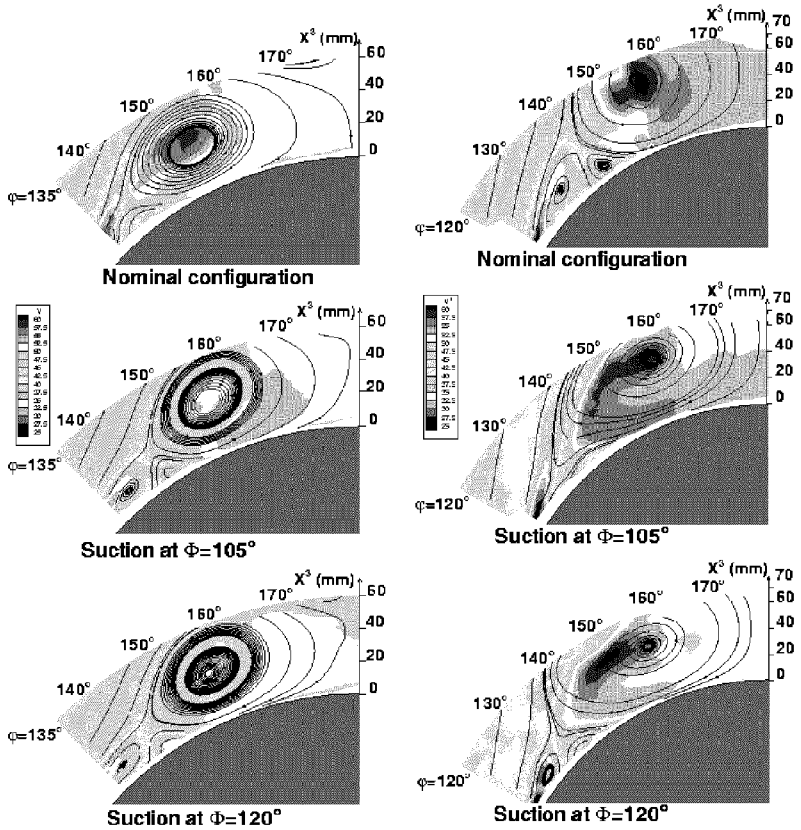


$XG^{I'}$=1060mm $XG^{I'}$=1300mm

Fig.17: Streamlines projection in the plane normal to the model longitudinal axis and longitudinal mean velocity component $\alpha$=30° , $V_0$=50m.s$^{-1}$ , Q=10m$^3$.h$^{-1}$ , $R_e$=5.6.10$^6$

low velocity region near the wall is eliminated. Therefore the secondary vortex and counter-vortex are no longer confined in this part of the flow and we observed a vertical extension of these two vortices structures. Further downstream, results shows significant differences with the previous plane.

Fig.17 on the right hand side shows the contours of the longitudinal mean velocity component and streamlines obtained for the nominal configuration, the configuration with suction at M = 105°, and the configuration with suction at M = 120° in the section at $XG^{1'}$ = 1300 mm. Now, for the nominal configuration, the development of a complex vortex structure is described by the projected streamlines. The main vortex near the leeward plane of symmetry must be completed by a secondary vortex and a counter vortex near the model wall. Application of suction does not change the position and magnitude of the main vortex but does alter the secondary and counter vortices.

## 5. CONTROL OF VORTEX BREAKDOWN BY ALONG THE CORE BLOWING

The delta wing configuration is a popular design choice for current military aircraft and missile systems expected to perform at high speeds and angles of attack. The increased lift is generated by multiple three-dimensional vortical structures in the flow field around a delta wing configuration. The prominent vortical structures are called *leading-edge vortices* and as $\alpha$ increases, these leading-edge vortices experience a sudden disorganisation, known as *vortex breakdown*. In general, vortex breakdown can be described by a rapid deceleration of both the axial and swirl components of the mean velocity and, at the same time, a dramatic expansion of the vortex core. During the breakdown process, the mean axial velocity component rapidly decreases until it reaches a stagnation point and/or becomes negative on the vortex axis. This stagnation point, identified as the *breakdown location*, is unsteady and typically oscillates about some mean position along the axis of the vortex core [10].

This research at ONERA by Mitchell *et. Al* [10,11,12] is examining along-the-core blowing as an effective method of controlling the vortex breakdown location over slender delta wings. In this study, open-loop, along the core blowing is used to manipulate the vortex breakdown location over the delta wing while the test configuration and freestream conditions remain constant. Results from laser sheet visualisation reveal the displacement of the vortex breakdown location under the influence of various blowing mass flow rates. The mean 3-D Laser Doppler Velocimetry (LDV) measurements within the vortical flow field and around the vortex breakdown are also discussed. The combined results demonstrate the influence of along-the-core blowing on the vortical flow field and the vortex breakdown locations.

A delta wing model with a 70° sweep angle ($\Lambda$) and root chord (c) of 950 mm has been configured to collect qualitative and quantitative surface and flow field data during these tests. The model has a wingspan of 691.5 mm at its trailing-edge, is 20 mm thick, and is bevelled on the windward side at an angle of 15° to form sharp leading-edge. The delta wing is equipped with a system of tubing which provides regulated compressed air to two nozzles located near the apex, which are symmetrically situated about the root chord. The nozzles are located 14% of the root chord downstream of the apex of the wing and are situated 30 mm from each leading-edge. Each nozzle consists of a circular jet which expands from an interior diameter of 2.07 mm into an open duct at an angle of 15.6° with respect to the leeward surface of the wing. The compressed air jet exits both nozzles slightly inward of the leading-edge vortex cores at supersonic exit velocities, based on isentropic relations and the measured total pressure of the compressed air, for all blowing mass flow rates considered in this study.

### 5.1. Results

All of the data presented in this paper was acquired at test conditions of $\alpha = 27°$ and $U_\infty = 24$ ($Re_c = 1.56 \times 10^6$). In the flow control study, along-the-core blowing mass flow rates were varied along each of the leading-edge vortices to compare their influence on the breakdown location of each vortex, controlled and uncontrolled. Blowing mass flow rates of 1.8, 2, 2.2, 3.3, and 3.7 g/s for each nozzle were studied during these tests. The influence of the flow control is determined by comparing the controlled flow results to the reference case, without blowing.

The vortex breakdown locations for the no-blowing and blowing configurations are determined from instantaneous video images from the laser sheet tests. (Fig.18) In these sample photographs, it is clear that the mean breakdown locations of both the portside and starboard vortices are not symmetrically situated over the wing. The results demonstrate the ability of the open-loop, along-the-core blowing to displace the vortex breakdown location toward the trailing edge of the wing. The effectiveness of the flow control to manipulate the controlled breakdown location is dependent on the blowing mass flow rate and the freestream velocity. As the blowing mass flow rates are increased, the effectiveness of the flow control improves and is more capable of displacing the vortex breakdown location further downstream. Due to the symmetry of the flow field over the leeward surface of the delta wing, with and without flow control, only the portside flow field of the delta wing is examined with LDV. Four planes perpendicular to the leeward surface of the wing and one longitudinal plane following the axis of the vortex core are explored. In the longitudinal plane, the portside leading-edge vortex is explored from X = 500 mm to X = 800 mm, with chordwise zones every 20 mm with meshes of 525 points. The location of the vortex core for the longitudinal plane was identified by the position of the maximum value of the axial velocity component (U) in the perpendicular plane measurements.

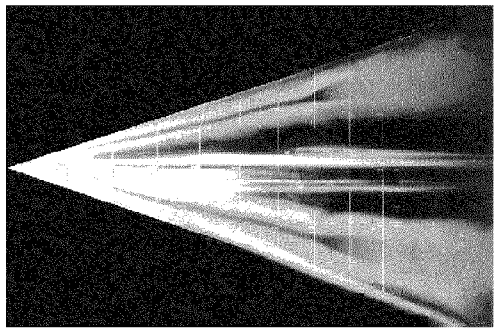

No flow control

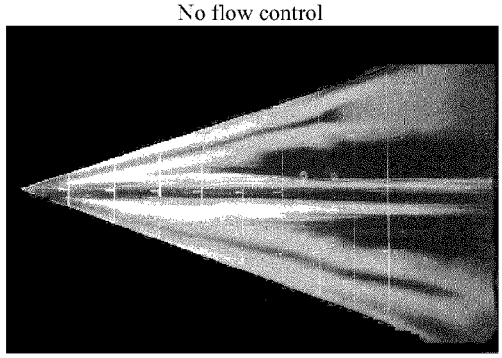

Flow control along lower vortex at $Q_m$ = 1.8 g/s.

Fig.18: $\alpha = 27°$, $U_\infty = 24$ m/s

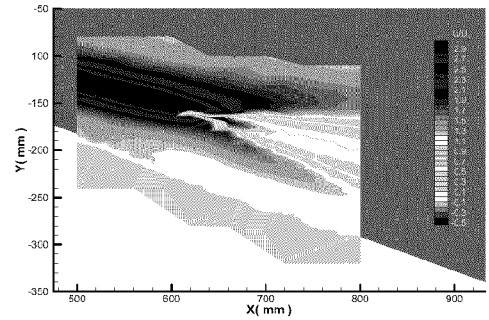


no flow control

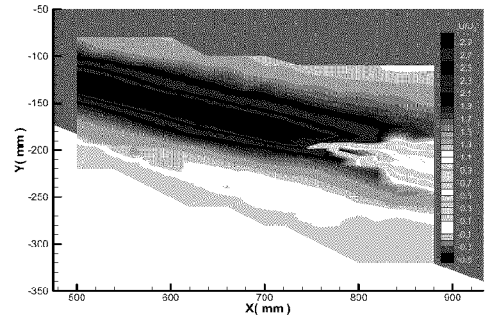


Along-the-core blowing with $Q_m$ = 1,8 g/s.

Fig.19: 3-D LDV results of $U/U_\infty$ in the longitudinal plane at $\alpha = 27°$ and $U_\infty = 24$ m.s$^{-1}$

Fig.19 presents the non-dimensional axial velocity component ($U/U_\infty$) in the longitudinal plane intersecting the leading-edge vortex cores. A strong, jet-like, acceleration of the flow along the vortex core is observed upstream of vortex breakdown phenomena ($X_b$ = 620 mm) with values of $U/U_\infty \geq 3.5$. There is an abrupt deceleration of the axial velocity component to a stagnation point (vortex breakdown location) which is followed by a zone of recirculation and a sizeable increase in the diameter of the vortex core. The post breakdown region has a wake-like axial velocity profile.

At locations upstream of the vortex breakdown, there are strong gradients of the vertical and horizontal components of the tangential velocity (V and W), indicating an intense rotation of the leading-edge vortex. Downstream of breakdown location these gradients diminish and the diameter of the vortex core expands. The results shown in Fig.19 indicate the effectiveness of along the core blowing in manipulating the vortex breakdown location downstream. The mean vortex breakdown location is displaced downstream at least 10% of the chord. These results compare well with those shown in Fig.18.

### 5.2. Conclusions

The ensemble of this data enabled the identification of the vortex breakdown location and provided characteristic details of the flow field and the vortex breakdown phenomena. Laser sheet visualisation enable identification of the vortex breakdown location and characterisation of its chordwise oscillation.

The 3-D LDV results verify the effectiveness of along the core blowing in manipulating the vortex breakdown location and reveal the physical changes that occur in the flow field and the vortical structures which cause the vortex breakdown location to be displaced aft. The LDV measurements provide a detailed description of the mean flow field in the vortex breakdown region.

Open-loop blowing along each of the leading-edge vortices on the leeward surface of the delta wing was examined. Both asymmetric and symmetric flow control configurations demonstrated the ability to displace the vortex breakdown location downstream toward the trailing edge of the delta wing. The ability of the various blowing configurations to manipulate the controlled breakdown location was dependent on the blowing mass flow rate and the freestream velocity. As the blowing mass flow rates increased, the effectiveness of the flow control improved and was more capable of delaying the vortex breakdown.

They confirm previous studies of the trends in the leading-edge vortices including the shift from a jet-like axial velocity profile upstream of the breakdown location to a wave-like profile. They are also used to identify the mechanism of the along core blowing which manipulates the vortex breakdown location. These results will allow for the development of more efficient flow control techniques and potentially a closed loop control system for vortex breakdown control.

## 6. CONCLUSION

In 1997, ONERA has decided to build a multidisciplinary project on aerodynamic active flow control. This project addresses several applications on which significant results have already be obtained.

On TS waves, it has been proven that active control is feasible, the next step, which has already started, consists in an extension to 3D including the control of the 3D steady waves that appear along the leading edge of a 3D wing.

On buffet control, 3D tests are on the way to be performed in the ONERA S2 Modane wind tunnel.

Closed loop control on vortex control will be performed before end the year 2000.

## 7. ACKNOWLEDGEMENT

The authors would like to express their sincerest thanks to the members of the F2 wind tunnel team for their help in accomplishing these tests.

## 8. REFERENCES

1- D.CARUANA, M.CORREGE, C.DESPRE, H.GASSOT,P.GIRODROUX-LAVIGNE, J.C.LE BALLEUR, A.MIGNOSI, O.REBERGA
Buffet Active Control - Experimental and Numerical Results
AVT SYMPOSIUM on Active Control Technology for Enhanced Performance Operation Capabilities of Military Aircraft, Land Vehicles and Sea Vehicles
Braunschweig, Germany, 8-11 May 2000

2- C.FRANÇOIS
Experimental Side Force Control on a Generic Forebody at High Angle of Attack
AVT SYMPOSIUM on Active Control Technology for Enhanced Performance Operation Capabilities of Military Aircraft, Land Vehicles and Sea Vehicles
Braunschweig, Germany, 8-11 May 2000

3- G.CASALIS
Instabilités primaire et secondaire dans la couche limite laminaire pour un fluide incompressible
Thèse de doctorat de l'Université de Paris 6 25 juin 1990

4- G.CASALIS, J.L.GOBERT, G.PAILHAS, S.PRUDHOMME
Active Control of TS Waves
Flow control - Fundamentals and Practices
Cargèse - Corsica 24 June-5 July 1996

5- D.BARBERIS, P.MOLTON, P.MALATERRE "
Control of 3D turbulent boundary layer separation caused by a wing-body junction " , Experimental Thermal and Fluid Sciences 16 (1998),pp.54-63.

6- KREPLIN H.P., MEIER H.U., and MAIER A.
"Wind Tunnel Model and Measuring Techniques for the Investigation of 3D Turbulent Boundary Layers," AIAA 10th Aerodynamic Testing Conference, San Diego, California, AIAA Paper 78-781, 1978.

7- RAYNAL J.C. and PELISSIER Ch.
"Essai dans la Soufflerie F1/CFM d'un Ellipsoïde de Révolution du DFVLR,"
ONERA Procés Verbal d'Essais 1/7252 ANG, 1983.

8- CHANETZ B.
"Contribution à l'Etude du Décollement 3D en Ecoulement Turbulent Incompressible,"
Thèse de Doctorat, ONERA NT - 1988-6, 1988.

9- BARBERIS D, MOLTON P.
" Experimental study of three-dimensional separation on a large-scale model"
AIAA Journal,Vol.33,No.11,
November 1995,pp.2107-2113.

10- MITCHELL A.M., BARBERIS D., DELERY J.
"Oscillation of Vortex Breakdown Location and Its Control by Tangential Blowing,"
AIAA-98-2914, AIAA 29th Fluid Dynamics Conference, Albuquerque, NM, June 1998.

11- MITCHELL A.M., MOLTON P., BARBERIS D., DELERY J.
" Control of Vortex Breakdown Location by Symmetric and Asymmetric Blowing"
AIAA-99-3652, 30th AIAA Fluid Dynamics Conference, Norfolk, VA, June 1999.

12- MITCHELL A.M., MOLTON P., BARBERIS D., DELERY J.
"Characterization of Vortex Breakdown by Flow Field and Surface Measurements"
AIAA-00-0788, 37th Aerospace Sciences Meeting and Exhibit, Reno, NV, Jan. 2000.

**This page has been deliberately left blank**

---

**Page intentionnellement blanche**